ELEVATIONAL SPATIAL COMPOUNDING

Pai-Chi Li and M. O'Donnell

Electrical Engineering and Computer Science Department
and Bioengineering Program
University of Michigan
Ann Arbor, MI 48109-2122

Spatial compounding has long been explored to reduce coherent speckle noise in medical ultrasound. By laterally translating a one-dimensional array, partially correlated measurements made at different look directions can be obtained and incoherently averaged. The lateral resolution, however, is limited by the sub-array length used for each independent measurement. To reduce speckle contrast without compromising lateral resolution, a new spatial compounding technique using two-dimensional, anisotropic arrays is proposed. This technique obtains partially correlated measurements by steering the image plane elevationally with small inclinations. Incoherent averaging is then performed by adding image magnitudes. Therefore, contrast resolution is improved only at the price of a slightly wider elevational beam. Note that although anisotropic arrays have limited steering capability in elevation, grating lobes are not considered influential since only small inclinations are needed between measurements. Simulations have been performed to show both the change in spatial resolution and the improvement in contrast resolution. Results indicated minimal increase in the correlation length both laterally and axially. It was also shown that detectability can be significantly enhanced by increasing the number of measurements or increasing the differential inclination between measurements. This technique is therefore effective for reducing speckle noise while maintaining in-plane spatial resolution. Furthermore, it demonstrates a new application of two-dimensional anisotropic arrays in spite of their limited elevational steering capability.   © 1994 Academic Press, Inc.

Key words: Anisotropic array; contrast resolution; detectability; spatial compounding; ultrasound imaging.

1. INTRODUCTION

Speckle is a common phenomenon in all coherent imaging systems. It arises from random interference of echoes backscattered from targets within the same resolution volume. Speckle appears as intensity variations imposed on the image, thus degrading inherent target detectability. In medical ultrasound, its mottled appearance masks acoustic properties of tissue, which provide true diagnostic values. It is therefore an undesired characteristic to be reduced.

The physical origin and statistics of speckle have long been studied [1-4]. Using a random walk model, the accumulation of random scattering during image formation can be described by the sum of a number of phasors. Each phasor is a complex number representing both the strength and phase (i.e., relative spatial position) of a scatterer.

176

If the number of phasors (i.e., the number of scatterers within a resolution volume) is sufficiently large, the image intensity becomes exponentially distributed. In other words, the acoustic signal-to-noise ratio (SNR), defined as the ratio of mean to standard deviation of the scattered signal, is unity. Therefore, speckle noise is signal dependent (i.e., noise power depends on local brightness) and acts like multiplicative noise.

Multiplicative noise filtering techniques have been proposed to reduce speckle [5-7]. They are not, however, particularly effective since the multiplicative noise model for speckle is only a rough approximation [8,9]. To fully characterize speckle and develop effective speckle reduction techniques, its spatial correlation, determined by the imaging system's point spread function, must be considered.

Compounding (i.e., incoherent averaging) techniques, such as spatial compounding, frequency compounding and temporal compounding, have been proposed for speckle reduction by introducing incoherence during image formation [10-18]. These techniques exploit the fact that the ensemble average of a speckle image is the same as the incoherent average of the original object. Hence, speckle variations are reduced by incoherently averaging partially correlated measurements without affecting the original intensity contrast. Speckle noise reduction results in an image with lower speckle fluctuations, i.e., an image with improved contrast resolution. The improvement, however, is usually gained at the price of spatial resolution.

Figure 1 illustrates the basic principles of spatial compounding with lateral array displacements (i.e., lateral spatial compounding). In this case, the sub-array with a length L_s is laterally translated N times ($N = 3$) by a distance d to obtain N independent measurements of the same region of interest (ROI). Incoherence is introduced due to the statistical independence of speckle viewed at different directions, and the correlation between measurements is primarily determined by the fractional aperture displacement. Depending on the coherence between measurements, speckle noise can be reduced by as much as $\sqrt{N}$ if N measurements are taken. Detailed analyses of speckle pattern correlation and optimum array displacement for efficient compounding can be found in [2, 11-13]. In addition to reducing speckle noise, lateral spatial compounding also provides better edge definition for specular targets. However, the lateral resolution is determined by the sub-aperture size (L_s) used for each measurement rather than the
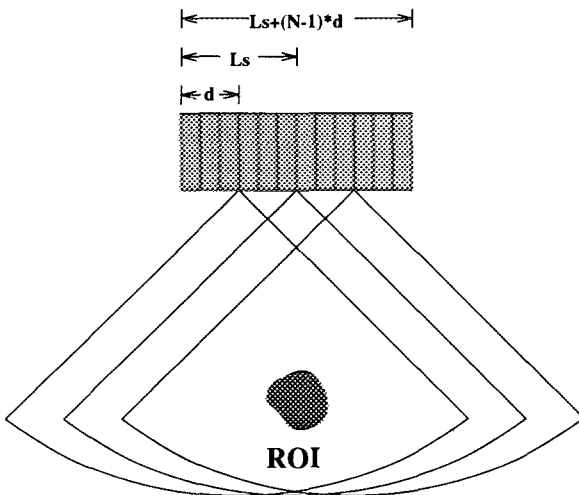

Fig. 1 Illustration of lateral spatial compounding (N=3).

overall aperture size $(L_s + (N-1) \cdot d)$. In other words, improvement in contrast resolution is compromised by reduced lateral spatial resolution.

Partially correlated measurements can also be obtained by other techniques. Frequency compounding, for example, divides the passband of input pulses into several sub-bands in the frequency domain [14–18]. Contrast resolution is therefore enhanced at the price of axial resolution due to the reduced pulse bandwidth. Similarly, temporal compounding sums intensities sampled at a higher rate [18]. Contrast resolution is also gained at the price of axial resolution.

All these techniques enhance contrast resolution by introducing incoherence either axially or laterally. To date, no techniques have been proposed to reduce speckle fluctuations by introducing incoherence in elevation, since one-dimensional arrays cannot steer in this direction. With the evolution of anisotropic, two-dimensional (i.e., 1.5 dimensional) arrays, compounding techniques exploiting elevational steering are of particular interest [19–24].

Very large, two-dimensional, anisotropic arrays have been proposed to reduce the size of the three-dimensional resolution volume, thus enhancing low contrast detectability as well as presenting fine spatial detail [25–28]. These arrays, undersampled in the non-scan direction to reduce total channel number, can produce a full three-dimensional focus. Due to the limited steering capability in elevation, however, they are not suitable for three-dimensional imaging. Nevertheless, potential applications of this limited steering capability should not be ignored. As shown in figure 2, these arrays can be used to obtain partially correlated or uncorrelated measurements by steering the image plane over small inclinations. Although grating lobes exist due to large interelement spacings in the non-scan direction, they are not considered influential since only small inclinations are needed for independent measurements. Therefore, contrast resolution can be improved without degrading in-plane (i.e., lateral and axial) spatial resolution. It is the goal of this paper to investigate elevational spatial compounding for anisotropic, two-dimensional arrays including theoretical correlation analysis and simulation verification.
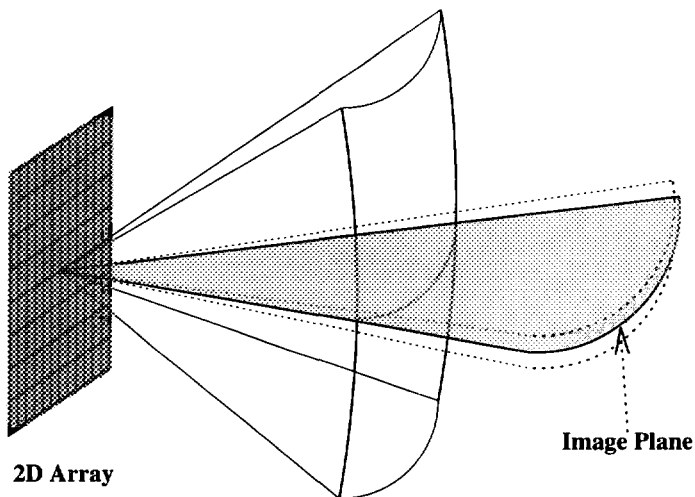

Fig. 2 Illustration of elevational spatial compounding.

The correlation between independent measurements is derived analytically in the next section. Simulation results, including qualitative image comparison and quantitative contrast resolution improvement, will be shown in section 3. Finally, this paper concludes in section 4 with a discussion of the results.

2. CORRELATION ANALYSIS

Assuming the imaging system has a linear, space invariant point spread function, an image can be obtained by convolving the point spread function with a scatterer distribution function. In other words, we have

$$s(\mathbf{u}) = \int_{-\infty}^{\infty} a(\mathbf{u} - \mathbf{u}')b(\mathbf{u}')d\mathbf{u}' \quad , \tag{1}$$

where $s(\cdot)$ is the image, $a(\cdot)$ is the scatterer distribution function and $b(\cdot)$ is the system's point spread function. All functions are complex and in a three-dimensional space denoted by $\mathbf{u} = (x, y, z)$. The complex cross-correlation function, $c(\mathbf{u}_1, \mathbf{u}_2)$, of two measurements, $s_1(\mathbf{u})$ and $s_2(\mathbf{u})$, is

$$c(\mathbf{u}_1, \mathbf{u}_2) \overset{def}{=} \langle s_1(\mathbf{u}_1)s_2^*(\mathbf{u}_2)\rangle = \int\int_{-\infty}^{\infty} \langle a(\mathbf{u}')a^*(\mathbf{u}'')\rangle \; b_1(\mathbf{u}_1 - \mathbf{u}')b_2^*(\mathbf{u}_2 - \mathbf{u}'')d\mathbf{u}'d\mathbf{u}'' \quad , \tag{2}$$

where $\langle\cdot\rangle$ represents the ensemble average, $b_1(\cdot)$ and $b_2(\cdot)$ represent the point spread functions for $s_1(\cdot)$ and $s_2(\cdot)$ respectively. Assuming the insonified region is fully developed speckle (i.e., it has a homogeneous distribution of scatterers with an average scattering strength a_0 and uncorrelated microscopic structures), the autocorrelation of the scatterer distribution function $a(\cdot)$ is

$$\langle a(\mathbf{u}')a^*(\mathbf{u}'')\rangle = a_0^2\delta(\mathbf{u}' - \mathbf{u}'') \quad , \tag{3}$$

where $\delta(\cdot)$ is the three-dimensional Dirac-delta function. Hence, Eq. (2) can be rewritten as

$$c(\mathbf{u}_1, \mathbf{u}_2) = a_0^2 \int_{-\infty}^{\infty} b_1(\mathbf{u}_1 - \mathbf{u}')b_2(\mathbf{u}_2 - \mathbf{u}')d\mathbf{u}' \quad . \tag{4}$$

Since a linear, space invariant point spread function is assumed, $b_1(\cdot)$ and $b_2(\cdot)$ are simply space shifted version of each other. In other words, $b_1(\mathbf{u}) = b(\mathbf{u}) = b_2(\mathbf{u} - \mathbf{u}_0)$, where $\mathbf{u}_0$ is the three-dimensional displacement between two measurements. Therefore, Eq. (4) becomes

$$c_s(\mathbf{u}_1 - \mathbf{u}_2) \overset{def}{=} c(\mathbf{u}_1, \mathbf{u}_2) = a_0^2 \int_{-\infty}^{\infty} b(\mathbf{u}_1 - \mathbf{u}')b(\mathbf{u}_2 - \mathbf{u}' + \mathbf{u}_0)d\mathbf{u}' \quad . \tag{5}$$

In other words, the correlation function $c_s(\mathbf{u}_1 - \mathbf{u}_2)$ depends on both the point spread function and the displacement between two measurements.

Coherence between images is often measured by the correlation coefficient, i.e., normalized coherence function. In other words, the cross-correlation function is evaluated at $(\mathbf{u}_1 - \mathbf{u}_2) = \mathbf{0} = (0, 0, 0)$. Therefore, we have

$$c_s(\mathbf{0}) = a_0^2 \int_{-\infty}^{\infty} b(\mathbf{u}_1 - \mathbf{u}')b(\mathbf{u}_1 - \mathbf{u}' - \mathbf{u}_0)d\mathbf{u}' = a_0^2 \int_{-\infty}^{\infty} b(\mathbf{u}''')b(\mathbf{u}''' - \mathbf{u}_0)d\mathbf{u}''' \quad . \tag{6}$$

The overall (two-way) point spread function is the product of transmit and receive responses, i.e., $b(\mathbf{u}) = b_t(\mathbf{u})b_r(\mathbf{u})$, where $b_t(\cdot)$ and $b_r(\cdot)$ are transmit and receive responses respectively. At the simultaneous focus of transmitter and receiver, $b_t(\mathbf{u}) = b_r(\mathbf{u})$ so that

$b(\mathbf{u}) = b_t^2(\mathbf{u})$. Assuming every image point is in focus, the three-dimensional point spread function becomes separable, i.e., $b_t(\mathbf{u}) = b_x(x)b_y(y)b_z(z)$, where $b_x(x)$, $b_y(y)$ and $b_z(z)$ represent the system's response in the lateral, elevational and axial direction respectively. The axial response $b_z(z)$ is simply the envelope of the wide band pulse used for insonification. Given an aperture, lateral and elevational beam patterns (i.e., $b_x(x)$ and $b_y(y)$) can also be obtained under the wide band condition. Without loss of generality, we assume here that the lateral and elevational patterns can be approximated by a continuous wave model. In other words, the beam patterns in these two directions are simply obtained by Fourier transforming the aperture function. Assuming a rectangular aperture, the lateral beam pattern is

$$b_x(x) = \frac{sin(x)}{x} \stackrel{def}{=} sinc(x) \tag{7}$$

$$x = \frac{\pi L sin\theta}{\lambda} \quad, \tag{8}$$

where L is the array length in the scan direction, θ is the azimuthal angle, and λ is the wavelength of the acoustic signal at the center frequency. Similarly, the elevational beam pattern can also be found as $b_y(y) = sinc(y)$, where $y = \frac{\pi H sin\phi}{\lambda}$. Here H is the array height in the non-scan direction and ϕ is the elevational angle. The two-way, three-dimensional point spread function is therefore the product of the transmit pattern and the receive pattern, i.e.,

$$b(\mathbf{u}) = sinc^2(x)sinc^2(y)b_z^2(z) \quad. \tag{9}$$

With elevational spatial compounding, the displacement between two measurements is only in the elevational direction. In other words,

$$\mathbf{u_0} = (0, y_0, 0) \tag{10}$$

$$y_0 = \frac{\pi H sin\phi_0}{\lambda} \quad, \tag{11}$$

where ϕ_0 is the inclination between two measurements. Therefore,

$$c_s(\mathbf{0}) = a_0^2 \int \int \int_{-\infty}^{\infty} sinc^4(x)sinc^2(y)sinc^2(y - y_0)b_z^4(z)dxdydz \quad. \tag{12}$$

Finally, the correlation coefficient (c.c.) is

$$c.c. \stackrel{def}{=} \frac{\langle s_1(\mathbf{u})s_2^*(\mathbf{u})\rangle}{[\langle|s_1(\mathbf{u})|^2\rangle\langle|s_2(\mathbf{u})|^2\rangle]^{\frac{1}{2}}} = k_0 \int_{-\infty}^{\infty} sinc^2(y)sinc^2(y - y_0)dy \quad, \tag{13}$$

where k_0 is a constant ensuring the correlation coefficient is unity if $y_0 = 0$.

As shown in the above equation, the correlation coefficient is determined only by the inclination (i.e., y_0) between measurements.

3. SIMULATION RESULTS

Images of a spherical, low contrast lesion made with a two-dimensional square array are simulated using a method similar to that described previously for one-dimensional arrays [27]. The array is densely sampled with 32 elements in the scan direction and coarsely sampled with 8 elements in the non-scan direction. In other words, the array element size in the non-scan direction is four times that in the scan direction. All im-

ages consist of a 128×128 grid where the vertical axis represents the axial direction and the horizontal axis azimuth, i.e., simulated images are in a sector format prior to scan conversion. In this format, dimensions of the point spread function are space invariant. Note that 128 beams in the lateral direction represent a 90° sector and 128 samples in the axial direction represent approximately a 10 mm distance at a 10 MHz sampling rate. All simulated lesions in this paper are centered on the array normal and are spherical in the unscan converted format. These lesions are approximately elliptic in a two-dimensional sector scan format. The envelope of the axial response has a Gaussian shape with a 35% fractional bandwidth. The lateral and elevational response, on the other hand, are simply obtained by Fourier transforming the aperture function, i.e., a continuous wave model is assumed. Although fundamental differences exist between continuous wave and wide band systems, general principles involved in simulating speckle patterns still hold.

To simulate speckle patterns, a random walk model is used where each step in the walk represents a received signal from a scatterer. Furthermore, the number of scatterers within a resolution volume is assumed large enough such that each image pixel can be characterized by a Rayleigh distributed magnitude and a uniformly distributed phase. Assuming a linear and space invariant point spread function, a speckle pattern is generated by convolving a two-way (transmit and receive), three-dimensional (lateral, elevational and axial) point spread function with a three-dimensional target pattern. Each pixel in this target pattern is a complex number with statistics as described above. On the other hand, the mean of the amplitude is a constant over the entire background and a different constant in the object. The ratio of these constants is a preselected local intensity variation. Since linear convolution is used, every pixel in the pattern is assumed in focus.

Figure 3 shows the correlation coefficient as a function of the inclination between two measurements. The solid line shows the results using Eq. (13) (i.e., correlation between two complex images) and the dashed line shows the correlation between two image magnitudes. The inclination in all examples is represented as a fraction of the one-way, *zero-crossing*, elevational beam width. Note that a zero-crossing beam width is defined as the width between the beam center and the first zero-crossing point in the continuous wave pattern. It is roughly 1.13 times the 6 dB beam width of a two-way beam pattern. From figure 3, it is shown that correlation between measurements decreases as the inclination increases. The correlation between two complex images, however, is higher than the correlation between two image magnitudes in all cases. Similar results have been previously reported [3].

One example of elevational spatial compounding is shown in figure 4. The left panel shows the original image of a spherical object with a 30 pixel radius (i.e., about 15° on each side of the array normal). The mean intensity in the sphere is only 5 dB lower than that in the background. The right panel shows the compound image with five measurements (compound image of five). Both images have a 20 dB display range. Note that for all the images in this paper, display dynamic range represents the thresheld signal dynamic range. The inclination between images is one half of the elevational beam width. Clearly, the texture becomes more uniform after compounding and the object becomes more detectable. In other words, contrast resolution is improved by reducing speckle variations.

More simulations are performed to further quantify the improvement in contrast resolution. Figure 5 shows the improvement in contrast-to-noise ratio (CNR) as a function of the number of measurements. CNR is defined as the ratio of the difference in mean intensity to the standard deviation of the speckle background on a logarithmic display [27], i.e.,

$$CNR \stackrel{def}{=} \frac{10\log_{10}(\frac{I_1}{I_2})}{\sigma} \quad , \tag{14}$$

where I_1 and I_2 are the mean intensities in background and lesion respectively, and σ is the standard deviation of the background. The standard deviation of a fully developed speckle pattern is 4.34 dB on a logarithmic display [27]. The inclination between two
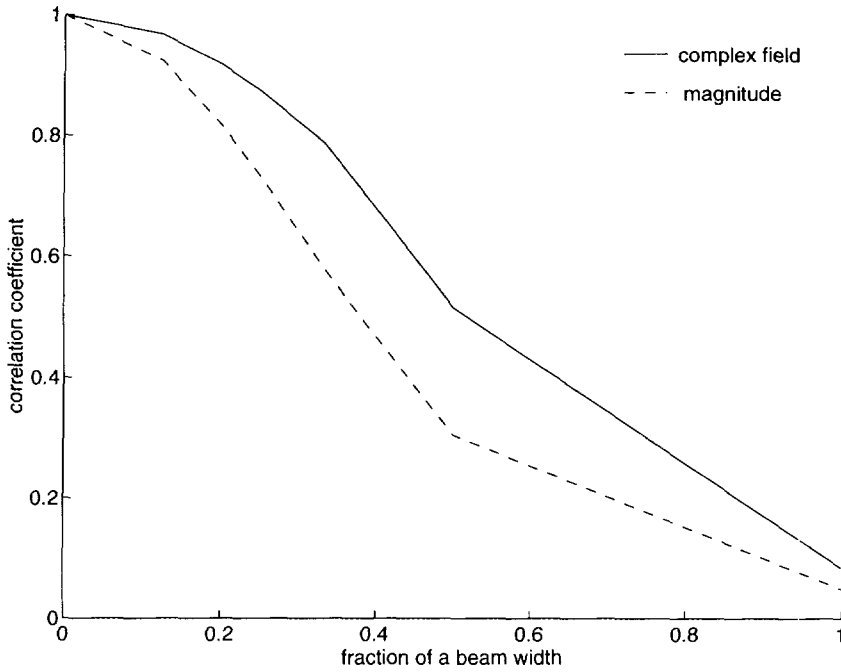
Fig. 3 Correlation coefficients between measurements.

adjacent images is one-seventh of the beam width. As expected, CNR increases as the number of images increases due to smaller texture variations (i.e., lower σ). Since the contrast is 5 dB between the object and the background, CNR for an "ideal" imager is $5/4.34 \approx 1.15$. Therefore, it is shown that CNR can surpass the "ideal" imager by applying elevational spatial compounding.

Figure 6 shows CNR as a function of inclination, expressed as the fraction of an elevational beam width. Clearly, CNR is improved by introducing incoherence between images as the inclination increases. After a certain inclination (one beam width), however, two images are considered uncorrelated and the correlation coefficient approaches zero. Therefore, the CNR cannot be further improved by increasing the differential inclination. Note that as the elevation increases, the two-dimensional slice area of the three-dimensional lesion on the image plane becomes smaller since a spherical object is assumed. This produces a smaller differential mean intensity, i.e., a smaller $\frac{I_1}{I_2}$. Therefore, the CNR with an inclination of 1.5 beam width is smaller than the CNR with an inclination of one beam width, although the noise power (i.e., σ) in both cases is very similar.

Autocorrelation functions of the image magnitudes are shown in figures 7 and 8 to illustrate the change in speckle cell size due to compounding. Figure 7 shows axial autocorrelation functions and figure 8 shows lateral autocorrelation functions. In both figures, the solid line represents the original image, the dot-dashed line depicts a compound image of three with a half beam width inclination between two adjacent measurements (com32) and the dashed line represents a compound image of five with the same inclination (com52). In both cases, the correlation length hardly changes after compounding,
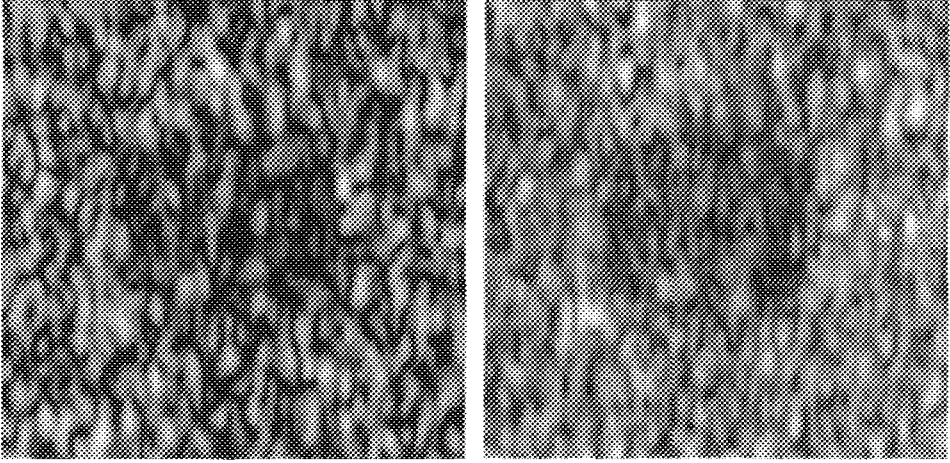
Fig. 4 Images of a spherical object with (right) and without (left) elevational spatial compounding.
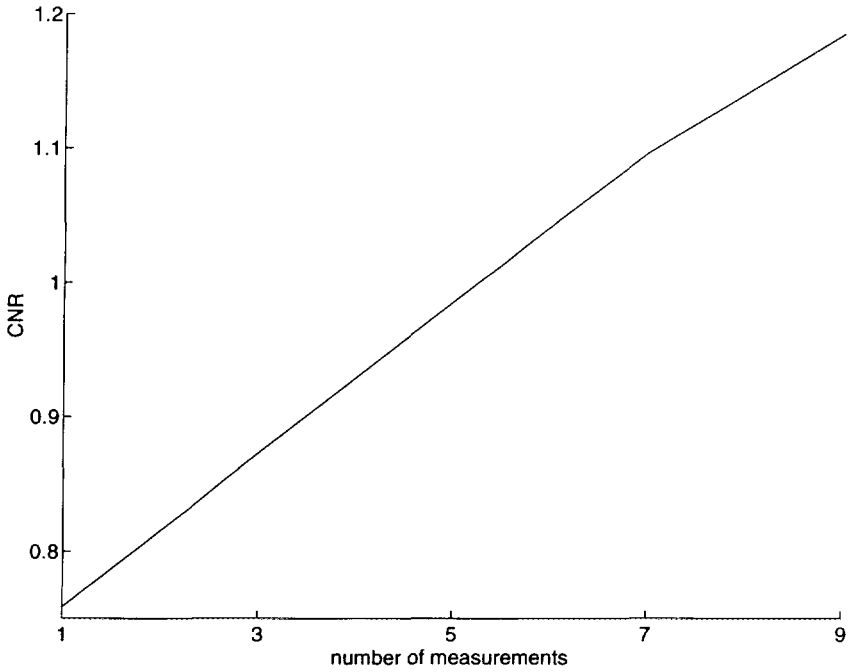

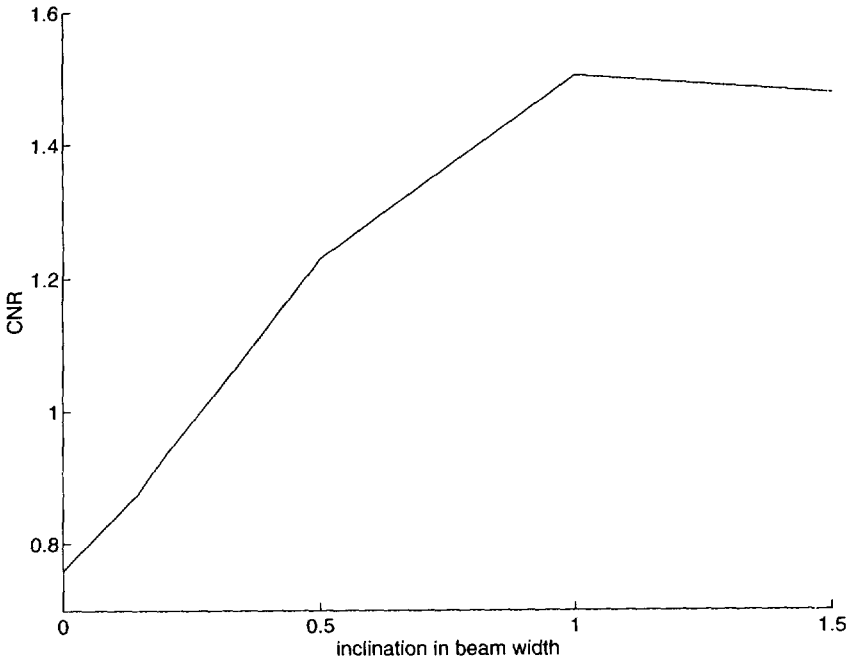Fig. 5 CNR as a function of the number of measurements.

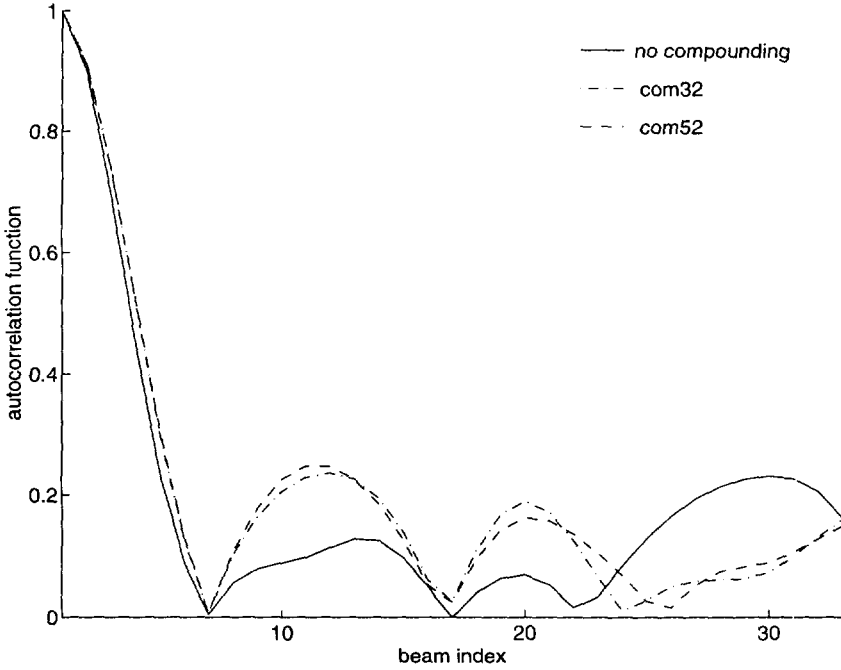Fig. 6 CNR as a function of inclination.

Fig. 7 Axial autocorrelation function with elevational spatial compounding.
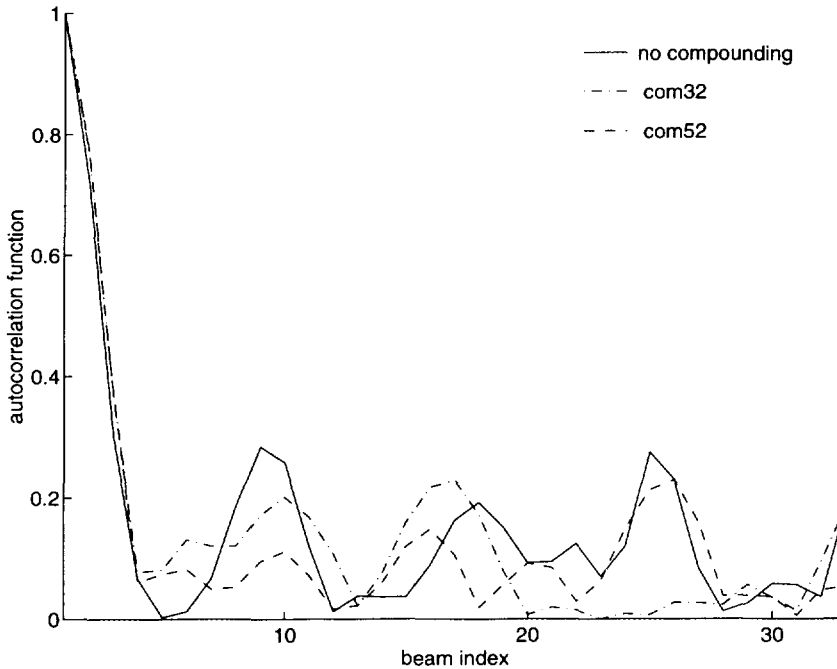
Fig. 8 Lateral autocorrelation function with elevational spatial compounding.

i.e., the speckle spot size does not change. Since the speckle spot size is determined by the point spread function, it is expected that two-dimensional spatial resolution is not influenced by elevational spatial compounding.

Changes in in-plane resolution are further illustrated in figure 9, where a three-dimensional point target is placed near the upper left corner in the image plane. The average background intensity is about 20 dB lower than the intensity of the point target and 5 dB higher than the average intensity inside the sphere. The left panel shows the original image and the right panel shows the compound image of five with a half beam width inclination. Both images have a 40 dB display dynamic range. Clearly, dimensions of the point spread function are not changed. The brightness, however, is reduced due to averaging since the point target is only present in the center image plane. With a "two-dimensional" point target (i.e., a wire), the average background brightness is expected to be the same.

A **maximum amplitude writing** technique using only the maximum amplitude of all measurements for each point is also investigated. It was shown that speckle contrast reduction with this technique is almost as large as incoherent averaging but bright point scatterers or specular reflectors are not lost [2]. Figure 10 contrasts images constructed with this method (right) to a noncompounded image (left) of the same object used in figure 9. Both images have a 40 dB display dynamic range and are normalized so that they have the same averaged background intensity. As expected, brightness reduction due to compounding can be avoided with this technique.
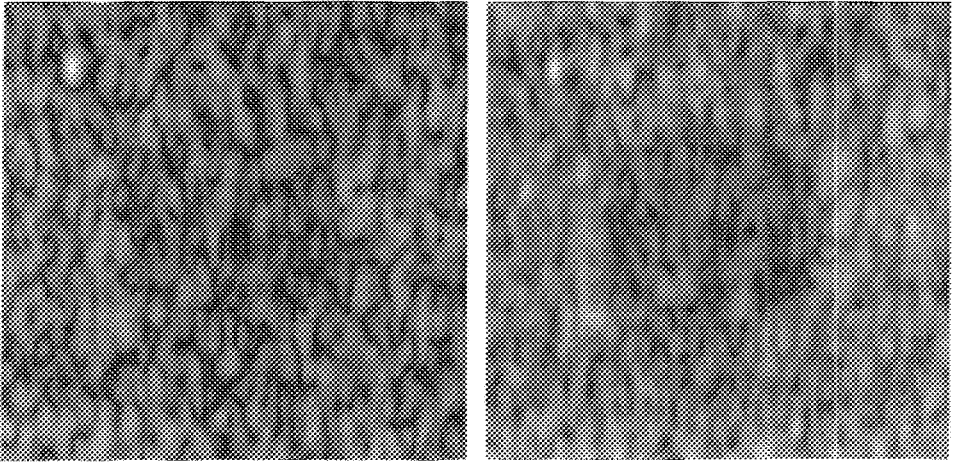
Fig. 9 Images of a spherical object and a point target with (right) and without (left) elevational spatial compounding.

4. DISCUSSION

In this paper, elevational spatial compounding for anisotropic, two-dimensional arrays has been presented. This technique exploits the limited steering capabil ty of these arrays to obtain independent measurements for incoherent averaging. Since inclinations
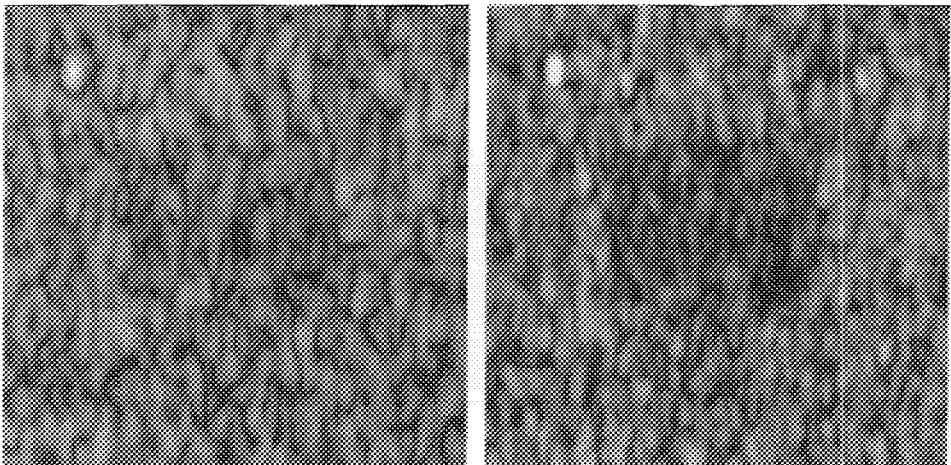

Fig. 10 Images of a spherical object and a point target with (right) and without (left) the maximum amplitude writing technique.

necessary for compounding are small, grating lobe effects of two-dimensional anisotropic arrays are not significant. Theoretical correlation analysis between two complex images has also been derived. It was compared to results using image magnitudes from simulations. The correlation between measurements was shown to decrease as the inclination increases. In addition, the correlation coefficient approaches zero if two images are over one elevational beam width apart. Simulation results also showed that this method can effectively improve contrast resolution without sacrificing **in-plane** spatial resolution. The improvement, however, is gained at the price of a slightly degraded elevational beam.

Large, two-dimensional arrays were originally proposed to improve the quality of three-dimensional focusing. With elevational spatial compounding, however, speckle reduction inevitably leads to loss in elevational spatial resolution. Note that the elevational beam width after compounding can be described by $(N - 1) * \theta + w_o$, where N is the number of measurements to be compounded, θ is the inclination between two adjacent measurements and w_o is the original beam width. In other words, the increase in elevational beam width is simply $(N - 1) * \theta$ assuming θ is sufficiently small (e.g., smaller than w_o). Nevertheless, unlike other methods, elevational compounding can reduce speckle variance without degrading in-plane spatial resolution. Ultimately, acceptance of this method as a clinical tool will depend on the specific imaging task.

In traditional compounding techniques using one-dimensional arrays, partially correlated measurements are made from the same object. Incoherence is introduced by measuring at different look directions, spectral components or temporal positions. Elevational spatial compounding, however, incoherently averages images of objects at slightly different spatial positions. Therefore, the inclination between measurements should be limited to avoid target misregistration. Misregistration can be further reduced using a maximum amplitude writing procedure originally proposed for mechanical B-scan systems.

The compounding technique can also be viewed as a spatial averaging technique which applies a **linear**, low-pass filter elevationally. On the other hand, the maximum amplitude writing technique performs a **non-linear**, rank-order filtering to reduce speckle variations. Due to the fundamental difference between this method and other compounding techniques, figure 3 not only describes the correlation between measurements to be compounded, it also represents the auto-correlation function of a single speckle target.

Elevational spatial compounding requires multiple scans for incoherent averaging. The image frame rate is therefore reduced. To maintain frame rate, parallel beamforming schemes can be employed. For example, a broader elevational beam or multiple foci pattern can be generated by array apodization or coded excitation on transmit. With parallel receive beamforming, elevational spatial compounding can be implemented without sacrificing image frame rate or restricting maximal range in the image. Possible performance degradation and increased hardware complexity must be further investigated.

Although the correlation between two complex images has been derived analytically, the direct relation between the correlation coefficient and CNR improvement is difficult to obtain for a general scattering object. In particular, if more than two measurements with small inclinations are used, interaction between nonadjacent measurements further complicates the analysis. Nevertheless, it is expected that CNR increases as the correlation between measurements decreases.

Finally, this paper shows an example of potential applications of two-dimensional anisotropic, or 1.5 dimensional, arrays. Although these arrays have limited elevational steering capability, other possible applications should be further explored.

ACKNOWLEDGMENTS

REFERENCES

[1] Goodman, J.W., Statistical Properties of Laser Speckle Patterns, in *Laser Speckle and Related Phenomena* (Springer-Verlag, Berlin, 1975).

[2] Burckhardt, C.B., Speckle in ultrasound B-mode scans, *IEEE Trans. Sonics Ultrason. 25*, 1-6 (1978).

[3] Wagner, R.F., Smith, S.W., Sandrik, J.M. and Lopez, H, Statistics of speckle in ultrasound B-scans, *IEEE Trans. Sonics Ultrason. 30*, 156-163 (1983).

[4] Smith, S.W., Wagner, R.F., Sandrik, J.M. and Lopez, H., Low contrast detectability and contrast/detail analysis in medical ultrasound, *IEEE Trans. Sonics Ultrason. 30*, 164-173 (1983).

[5] Lim, J.S. and Nawab, H., Techniques for speckle noise removal, *Opt. Engin. 20*, 472-480 (1981).

[6] Lee, J.S., Speckle analysis and smoothing of synthetic aperture radar images, *Comp. Graphics. Image Process. 17*, 24-32 (1981).

[7] Frost, V.S., Stiles, J.A., Shanmugan, K.S. and Holtzman, J.C., A model for radar images and its application to adaptive digital filtering for multiplicative noise, *IEEE Trans. Pattern Anal. and Machine Intelligence 4*, 157-166 (1982).

[8] Tur, M., Chin, K.C. and Goodman, J.W., When is speckle noise multiplicative, *Applied Optics 21*, 1157-1159 (1982).

[9] Kuan, D.T., Sawchuk, A.A., Strand, T.C. and Chavel, P., Adaptive restoration of images with speckle, *IEEE Trans. Acoust., Speech, and Signal Processing 35*, 373-383 (1987).

[10] Shattuck, D.P. and von Ramm, O.T., Compound scanning with a phased array, *Ultrasonic Imaging 4*, 93-107 (1982).

[11] O'Donnell, M., and Silverstein, S.D., Optimum displacement for compound image generation in medical ultrasound, *IEEE Trans. Ultrason, Ferroelec., Freq. Contr. 35*, 470-476 (1988).

[12] Silverstein, S.D. and O'Donnell, M., Speckle Reduction Using Correlated Mixed-Integration Techniques, in *SPIE 768 Pattern Recognition and Acoustical Imaging*, pp. 168-172 (SPIE, Bellingham, 1987).

[13] Trahey, G.E., Smith, S.W., von Ramm, O.T., Speckle pattern correlation with lateral aperture translation: experimental results and implications for spatial compounding, *IEEE Trans. Ultrason., Ferroelec., Freq. Contr. 33*, 257-264 (1986).

[14] Magnin, P.A., von Ramm, O.T. and Thurstone, F.L., Frequency compounding for speckle contrast reduction in phased array images, *Ultrasonic Imaging 4*, 267-281 (1982).

[15] Gehlbach, S.M., *Pulse reflection imaging and acoustic speckle*, Thesis Dissertation, Stanford University (1983).

[16] Melton, H.E., Jr. and Magnin, P.A., A-mode speckle reduction with compound frequencies and compound bandwidths, *Ultrasonic Imaging 6*, 159-173 (1984).

[17] Trahey, G.E., Allison, J.W., Smith, S.W. and von Ramm, O.T., A quantitative approach to speckle reduction via frequency compounding, *Ultrasonic Imaging 8*, 151-164 (1986).

[18] Silverstein, S.D., and O'Donnell, M., Frequency and Temporal Compounding of Partially Correlated Signals: Speckle Suppression and Image Resolution, in *SPIE 845 Visual Communications and Image Processing II*, pp. 188-194 (SPIE, Bellingham, 1987).

[19] Takeuchi, H., Masuzawa, H., Nakaya, C. and Ito, Y., Medical Ultrasonic Probe Using Electrostrictive Ceramics/Polymer Composite", in *Proceedings of the 1989 IEEE Ultrasonics Symposium*, pp. 705-708, IEEE Cat. No. 89CH2791-2 (IEEE, New York, 1989).

[20] Takeuchi, H., Masuzawa, H. and Nakaya, C., Relaxor Ferroelectric Transducers, in *Proceedings of the 1990 IEEE Ultrasonics Symposium*, pp. 697-705, IEEE Cat. No. 90CH2938-9 (IEEE, New York, 1990).

[21] Smith, L.S., Engeler, W.E., O'Donnell, M. and Piel, J.E., Jr., Rectilinear Phased Array Transducer Using 2-2 Ceramic-Polymer Composite, in *Proceedings of the 1990 IEEE Ultrasonics Symposium*, pp. 805-808, IEEE Cat. No. 90CH2938-9 (IEEE, New York, 1990).

[22] Daft, C.M.W., Smith, S. and O'Donnell, M., Beam Profiles and Images from Two-Dimensional Arrays, in *Proceedings of the 1990 IEEE Ultrasonics Symposium*, pp. 775-779, IEEE Cat. No. 90CH2938-9 (IEEE, New York, 1990).

[23] Smith, W.A., New Opportunities in Ultrasonic Transducers Emerging from Innovations in Piezoelectric Materials, in *SPIE 1733 New Developments in Ultrasonic Transducers and Transducer Systems*, pp. 3-26 (SPIE, Bellingham, 1992).

[24] Thomas, L., Wildes, D., Smith, L.S., Daft, C.M.W. and Rigby, W., Current Status and Future Prospects for High Channel Count Ultrasonic Imagers, *the 36th Annual Meeting and Exhibition of American Association of Physicists in Medicine*, (AAPM, Anaheim, 1994).

[25] O'Donnell, M. and Li, P.-C., Aberration Correction on a Two-dimensional Anisotropic Phased Array, in *Proceedings of the 1991 IEEE Ultrasonics Symposium*, pp. 1189-1193, IEEE Cat. No. 91CH3079-1 (IEEE, New York, 1991).

[26] Li, P.-C., Flax, S.W., Ebbini, E.S. and O'Donnell, M., Blocked element compensation in phased array imaging, *IEEE Trans. Ultrason., Ferroelec. Freq. Contr. 40*, 283-292 (1993).

[27] Li, P.-C. and O'Donnell, M., Improved detectability with blocked element compensation, *accepted for publication in Ultrasonic Imaging (1994)*.

[28] Li, P.-C. and O'Donnell, M., Phase aberration correction on two-dimensional conformal arrays, *accepted for publication in IEEE Trans. Ultrason., Ferroelec. Freq. Contr. (1993)*.